Linear global stability of a downward flow of liquid metal in a vertical duct under strong wall heating and transverse magnetic field

Jun Hu *

Laboratory of Computational Physics, Institute of Applied Physics and Computational Mathematics, P.O. Box 8009, Beijing 100088, China

(Received 3 April 2021; accepted 25 June 2021; published 21 July 2021)

The linear global stability of a downward flow of liquid metal in a vertical duct under strong wall heating and a transverse magnetic field is examined numerically. The two-dimensional steady-state magnetohydrodynamic (MHD) mixed convection with an upward reverse flow is first computed by the finite-element method. Then linear global stability equations of the MHD mixed convection are derived and solved by the spatial discretization of the Taylor-Hood finite element and an implicitly restarted Arnoldi algorithm for the resulted generalized eigenvalue problem. Elevator and oscillatory unstable modes are revealed through the eigenspetrum computation of linear global stability equations. The elevator mode is found to be always unstable and independent of the basic flow profile, though a large magnetic field may suppress its growth rate. The unstable oscillatory mode is directly related to the basic upward reverse flow and first occurs at the specific flow structure which has an upward reverse flow near the heating wall and a downward flow near the opposite wall. The critical curves of the Grashof number with respect to the Hartmann number for the three-dimensional oscillatory mode are plotted and reveal that larger Hartmann numbers have larger critical Grashof numbers. Energy budget analyses are also performed and show that the shear Kelvin-Helmholtz instability due to the existence of an inflection point is the key instability mechanism of the three-dimensional oscillatory mode. The appearance of the unstable oscillatory mode may be regarded as an alternative physical explanation of the high-amplitude, low-frequency pulsations of temperature in the experiments and related numerical simulations.

DOI: 10.1103/PhysRevFluids.6.073502

I. INTRODUCTION

Liquid metal flows in ducts and manifolds under a large heat flux and strong magnetic field are closely relevant to the design of liquid metal blankets of magnetic-confinement nuclear fusion reactors (tokamak or stellarator). Liquid metal blankets can provide three key functions with heat exchangers, radiation shields, and tritium breeders at the same time and are believed to be the most promising candidates for future fusion reactors [1–5]. Magnetohydrodynamics (MHD) [6] in liquid metal duct flows involves the study of the motion and evolution of electrically conducting fluids in the presence of magnetic fields. Conventionally without considering the thermal effect, the action of a magnetic field on a flow of an electrically conducting fluid can profoundly change flow behavior and produce a rich variety of phenomena [7–9] which have attracted extensive scientific interest. On the one hand, the magnetic field can lead to a change of the laminar-turbulent transition mechanism [10,11] in MHD flows. The magnetic field usually tends to suppress the production of turbulence and make the transition from laminar flow to turbulence occur at a much higher Reynolds

*hu_jun@iapcm.ac.cn

number [12]. The laminar-turbulent transition in MHD duct, pipe, and channel flows has been reviewed comprehensively by Zikanov *et al.* [13], with important experimental and computational results. On the other hand, many specific spatial structures such as shear layers [14], inflexion points [15], and jets [16] may appear in MHD flows due to the action of the magnetic field and can produce instabilities of the free shear flow type. For instance, the sidewall jets appearing in the MHD duct flow with perfectly or thin conducting rectangular walls [17–19] may produce linear instability under a strong transverse magnetic field. Then the critical Reynolds number of jet-induced instability appears to be significantly lower than the Reynolds numbers at which turbulence is observed in experiments [20] or direct numerical simulations [21].

In various design concepts of liquid blankets, the heat flux effect is an unavoidable consideration and may give rise to thermal convection instabilities which make magnetohydrodynamics more complicated. The thermal convection mechanism leads to the development of large-scale coherent structures which have been demonstrated in experiments by Genin *et al.* [22] and Belyaev *et al.* [23] for liquid metal flows in a heated horizontal tube under a transverse horizontal magnetic field. It was found that temperature fluctuations disappeared at moderately strong magnetic fields but reappeared at stronger magnetic fields in the form of anomalous high-amplitude, low-frequency temperature fluctuations. Thus hydrodynamic instabilities are supposed to play a key role in the appearance of these coherent structures and are verified by direct numerical simulations [24,25] and recent linear global stability analyses [26]. High-amplitude, low-frequency pulsations of temperature in the form of isolated bursts or quasiregular fluctuations have also been observed in experiments [27–31] on a downward flow in a vertical round pipe and rectangular duct with one wall heated and an imposed strong magnetic field. These temperature pulsations are also explained by the hydrodynamic instabilities due to the appearance of reversed flow and then the existence of the inflection point of the streamwise velocity near the heated wall in numerical simulations [31,32]. The high-amplitude, low-frequency fluctuations of velocity and temperature that appear in horizontal or vertical duct flows with strong heat flux and magnetic field effects are called magnetoconvective fluctuations [33] and have been reviewed recently by Zikanov *et al.* [34].

As for stabilities of the mixed thermal convections in the horizontal or vertical duct with one wall heated and a strong transverse magnetic field, the quasi-two-dimensional (Q2D) model proposed by Sommeria and Moreau [35] is usually adopted through describing the flow variables, such as velocity and temperature, integrated wall to wall in the magnetic field direction. Based on purely two-dimensional governing equations of the Q2D model, Smolentsev *et al.* [36] first studied instabilities and transitions in MHD duct flows with a symmetric "M-shaped" velocity profile by imposing an external flow-opposing force. Various instability modes and transition scenarios have been revealed by varying this external force and position of the inflection point. Vetcha *et al.* [37] considered the upward flows in a vertical rectangular duct subject to volumetric heating and a strong transverse magnetic field. Both bulk instability associated with the inflection point and sidewall boundary layer instability are predicted by their linear stability analysis. Vo *et al.* [38] investigated the linear stability of horizontal Poiseuille-Rayleigh-Bénard flows subjected to a transverse magnetic field and a vertical temperature gradient. Liu and Zikanov [39] further investigated the elevator convection mode for the vertical downward flow through the Q2D model. Zikanov and Listratov [40] performed numerical simulations of the downward flow of a liquid metal in a vertical pipe and attributed the high-amplitude fluctuations of temperature to the growth and quasiperiodic breakdown of the pairs of ascending and descending jets related to the elevator modes. Using the Q2D model, Zhang and Zikanov [32] numerically investigated the stabilities of the downward flow in a vertical duct with one heated and three thermally insulated walls under a strong transverse magnetic field. The downward flow is found to be steady state or oscillating depending on the strengths of the heating and magnetic field.

The Q2D model is originally proposed in the limit of a high interaction parameter ($\mathrm{Ha}^2/\mathrm{Re} \gg 1$) and Hartmann number ($\mathrm{Ha} \gg 1$). Thus it is not suitable for study of the hydrodynamic stabilities of MHD duct flows in full physical parameter space, especially to detect the instability boundary when the unstable threshold occurs at a much lower interaction parameter and Hartmann number. Even at

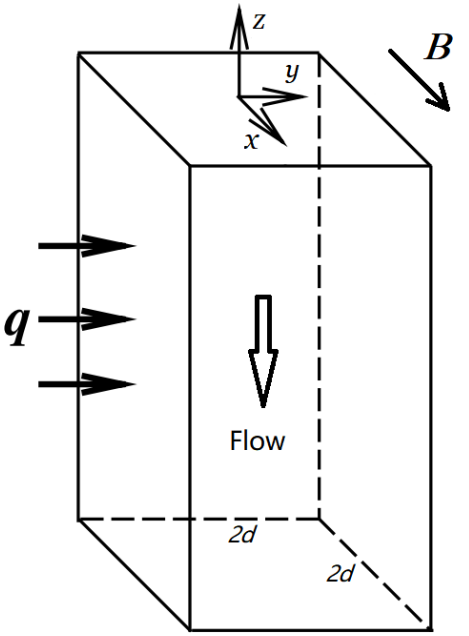

FIG. 1. Flow configuration for liquid metal flowing downward in a vertical duct under one-wall heating and a transverse magnetic field.

a high Hartmann number, for the mixed convection in a horizontal duct with an imposed transverse horizontal magnetic field, the applicability of the Q2D model is not *a priori* certain due to the numerical discovery of a large-scale coherent structure [25] which has significant flow and variations of temperature along the magnetic field lines in the high-Grashof regime. Furthermore, the full linear stability analysis of horizontal mixed MHD convection has revealed that the instability thresholds of steady solutions with symmetrical or asymmetrical rolls occur at a much lower Hartmann number and Grashof number [26]. This clearly shows that the Q2D model is not appropriate for research on the occurrence process or mechanism of stabilities of the mixed thermal MHD convections in the horizontal duct. It should also be realized that linear stabilities of a downward flow of liquid metal in a vertical duct under strong wall heating and a transverse magnetic field should be performed through the original governing equations without using the Q2D model. In this paper, full linear stability analyses without the Q2D approximation for such downward mixed convection flows are accomplished successfully. First, the two-dimensional steady-state flow with an upward reverse flow is computed by the finite-element method. Then three-dimensional linear stability equations of MHD mixed convection are derived and discretized spatially by the Taylor-Hood finite element. The resulting generalized eigenvalue problem is solved by an implicitly restarted Arnoldi algorithm with the shift-and-invert strategy. The obtained eigenvalues and corresponding eigenfunctions are directly used for the accurate determination of the linear stability boundary and the destabilization mechanism of the MHD mixed convection through energy budget analyses. Through the above linear stability computations and analyses, two unstable modes, i.e., the elevator mode and oscillatory mode, are revealed, and their destabilization characteristics are described in detail.

II. PHYSICAL MODEL AND GOVERNING EQUATIONS

A downward flow of liquid metal in a vertical duct is subjected to one-sidewall heating with heat flux intensity q and an external constant transverse magnetic field $\mathbf{B}_0(= B_0\mathbf{e}_x)$, as shown in Fig. 1.

The liquid metal is assumed to be an incompressible, electrically conducting Newtonian viscous fluid and homogeneous with regard to its physical properties such as a constant kinematic viscosity ν, thermal conductivity κ, and electric conductivity σ. There exist two main approximations usually used in numerical and theoretical research on the mixed convection in pipe and duct flows with strong magnetic fields [34]. One is the Oberbeck-Boussinesq approximation for the representation of buoyancy force, i.e., the density of fluid metal is assumed to vary linearly with the temperature in the buoyancy force term,

$$\mathbf{F}_b = (\rho - \rho_0)\mathbf{g}, \quad \rho = \rho_0[1 - \beta(T - T_0)]. \tag{1}$$

Here, ρ is the fluid mass density, T is the fluid temperature, β is the thermal expansion coefficient, $\mathbf{g}$ is the gravity acceleration in the negative z direction, and the subscript 0 is denoted as a reference value.

Another approximation is the quasistatic model, which has been proven to be accurate enough when the magnetic Reynolds and Prandtl numbers are both small [7,9]. In most laboratory experiments, the magnetic Reynolds number is relatively small and the induced magnetic field is much weaker than the imposed field. Then the quasistatic model assumes that the induced magnetic field can be neglected and the magnetic field remains almost undisturbed in the expressions of Ohm's law and the Lorentz force, which are formulated as follows:

$$j = \sigma(-\nabla\phi + v \times \mathbf{B}_0), \tag{2}$$

$$\mathbf{F}_l = j \times \mathbf{B}_0. \tag{3}$$

Here, ϕ is the electrostatic potential, and j is the induced electric current density. The current density can be considered to be solenoidal by neglecting displacement currents and assuming the fluid to be electrically neutral, i.e.,

$$\nabla \cdot j = 0. \tag{4}$$

Then by substituting Ohm's law into the above solenoidal relation, a Poisson equation for the electrostatic potential is obtained as follows:

$$\nabla^2\phi = \nabla \cdot (v \times \mathbf{B}_0). \tag{5}$$

Considering both the buoyancy force and the Lorentz force with the above two approximations, the governing equations for the liquid metal duct flow can be described by the Navier-Stokes system

$$\rho_0\left[\frac{\partial v}{\partial t} + v \cdot \nabla v\right] = -\nabla p + \rho_0 \nu \nabla^2 v + \mathbf{F}_b + \mathbf{F}_l, \tag{6}$$

$$\nabla \cdot v = 0. \tag{7}$$

By neglecting the Joule and viscous dissipations as well as other sources of volumetric energy release like nuclear radiation and chemical reactions, the convection diffusion equation derived from the energy balance can be formulated with the temperature T of the form

$$\frac{\partial T}{\partial t} + v \cdot \nabla T = \chi \nabla^2 T. \tag{8}$$

Here, $\chi = \kappa/\rho c_p$ is the thermal diffusivity, c_p is the specific heat capacity, and κ the thermal conductivity.

The boundary conditions on the heating sidewall include a nonslip condition for the velocity and a constant heat flux for the temperature, i.e.,

$$-\kappa\frac{\partial T}{\partial y} = q, \tag{9}$$

and the boundary conditions for the other three sidewalls are nonslip and thermal insulated, i.e.,

$$\frac{\partial T}{\partial n} = 0. \tag{10}$$

The dimensional governing equations can be further nondimensionalized by using the duct half-width d as the length scale, the mean streamwise velocity U_m as the velocity scale, qd/κ as the temperature scale, B_0 as the scale of the magnetic field strength, and dBU_m as the scale of the electric potential. Then the dimensionless governing equations can be written as

$$\frac{\partial v}{\partial t} + v \cdot \nabla v = -\nabla p + \frac{1}{\mathrm{Re}}\nabla^2 v + \mathbf{f}_b + \mathbf{f}_l, \tag{11}$$

$$\nabla \cdot v = 0, \tag{12}$$

$$\frac{\partial T}{\partial t} + v \cdot \nabla T = \frac{1}{\mathrm{Pe}}\nabla^2 T. \tag{13}$$

The boundary conditions at the duct walls are the no-slip conditions for velocity,

$$v = 0 \quad \text{at} \quad x = \pm 1, \quad y = \pm 1, \tag{14}$$

and perfect electric insulation,

$$\frac{\partial \phi}{\partial n} = 0, \tag{15}$$

and temperature conditions of constant heat flux at the heating wall and thermal insulation at the other three sidewalls,

$$\frac{\partial T}{\partial n} = -1 \quad \text{at} \quad y = -1, \tag{16}$$

$$\frac{\partial T}{\partial n} = 0 \quad \text{at} \quad y = 1, \tag{17}$$

$$\frac{\partial T}{\partial n} = 0 \quad \text{at} \quad x = \pm 1. \tag{18}$$

The buoyancy and Lorentz forces are dimensionalized as

$$\mathbf{f}_b = \frac{\mathrm{Gr}}{\mathrm{Re}^2} T \mathbf{e}_z \quad \text{and} \quad \mathbf{f}_l = \frac{\mathrm{Ha}^2}{\mathrm{Re}} j \times \mathbf{e}_x, \tag{19}$$

where the dimensionless parameters including the Reynolds number, Prandtl number, Péclet number, Grashof number, and Hartmann number are defined as

$$\mathrm{Re} = \frac{U_m d}{\nu}, \quad \mathrm{Pr} = \frac{\nu}{\chi} \quad \mathrm{Pe} = \frac{U_m d}{\chi} = \mathrm{Re} \cdot \mathrm{Pr}, \tag{20}$$

$$\mathrm{Gr} = \frac{g\beta q d^4}{\nu^2 \kappa}, \quad \mathrm{Ha} = B_0 d \left(\frac{\sigma}{\rho_0 \nu} \right)^{1/2}. \tag{21}$$

The temperature field can be further decomposed as the sum of the mean mixed temperature and the resulting temperature deviation:

$$T(\mathbf{x}, t) = T_m(z) + \theta(\mathbf{x}, t). \tag{22}$$

The mean temperature T_m is assumed to be a linear function of the streamwise coordinate z which makes the overall energy balance between the wall heat flux and the heat transport by the streamwise mean velocity. Then its streamwise gradient is given by

$$\frac{dT_m}{dz} = -\frac{\mathrm{P}}{A \cdot \mathrm{Pe}}, \tag{23}$$

where $\mathrm{P} = 2$ is the perimeter of the heated portion of the wall and $A = 4$ is the cross-sectional area of the square duct. Thus the temperature governing equation is written as

$$\frac{\partial \theta}{\partial t} + v \cdot \nabla \theta = \frac{1}{\mathrm{Pe}} \nabla^2 \theta - w \frac{dT_m}{dz}. \tag{24}$$

The pressure can also be decomposed into three parts as follows:

$$p = \tilde{p}(z) + \check{p}(z) + p(\mathbf{x}, t). \tag{25}$$

The first time-independent part is a quadratic parabolic function of z which balances the buoyancy force from the mean temperature, i.e.,

$$\frac{d\tilde{p}}{dz} = \frac{\mathrm{Gr}}{\mathrm{Re}^2} T_m. \tag{26}$$

The second part is a linear function of z which is used to drive the duct flow. The third part is the time-dependent pressure deviation, thus the momentum equation is reduced to

$$\frac{\partial v}{\partial t} + v \cdot \nabla v = -\nabla p - \nabla \check{p} + \frac{1}{\mathrm{Re}} \nabla^2 v + \frac{\mathrm{Gr}}{\mathrm{Re}^2} \theta \mathbf{e}_z + \frac{\mathrm{Ha}^2}{\mathrm{Re}} j \times \mathbf{e}_x. \tag{27}$$

In the steady-state solutions it is assumed that the velocity, pressure deviation, temperature deviation, and electrostatic potential are independent of the time and streamwise coordinate, as follows:

$$v_b = V(x, y) = (\overrightarrow{U}(x, y), W(x, y)), \tag{28}$$

$$p = P(x, y), \quad \theta = \Theta(x, y), \quad \phi = \Phi(x, y). \tag{29}$$

Here, $\overrightarrow{U} = (U, V)$ is the cross-sectional velocity, and W is the streamwise velocity. Thus the two-dimensional steady governing systems for the steady flow state are obtained as follows:

$$(\overrightarrow{U} \cdot \nabla_s) W = -d\check{p}/dz + \frac{\mathrm{Gr}}{\mathrm{Re}^2} \Theta + \frac{1}{\mathrm{Re}} \nabla_s^2 W + \frac{\mathrm{Ha}^2}{\mathrm{Re}} F_z, \tag{30}$$

$$(\overrightarrow{U} \cdot \nabla_s) \overrightarrow{U} = -\nabla_s P + \frac{1}{\mathrm{Re}} \nabla_s^2 \overrightarrow{U} + \frac{\mathrm{Ha}^2}{\mathrm{Re}} \overrightarrow{f}, \tag{31}$$

$$(\overrightarrow{U} \cdot \nabla_s) \Theta = \frac{1}{\mathrm{Pe}} \nabla_s^2 \Theta - W \frac{dT_m}{dz}, \tag{32}$$

$$\nabla_s \cdot \overrightarrow{U} = 0, \tag{33}$$

$$\overrightarrow{F} = (-\nabla \Phi + v_b \times \mathbf{e}_x) \times \mathbf{e}_x, \tag{34}$$

$$\nabla^2 \Phi = \nabla \cdot (v_b \times \mathbf{e}_x). \tag{35}$$

Here, $\nabla_s = (\partial_x, \partial_y)$, $\overrightarrow{F} = (\overrightarrow{f}, F_z)$, and $\overrightarrow{f} = (F_x, F_y)$. If the cross-sectional velocity $\overrightarrow{U}$ is set to 0, the governing equations for the steady-state solutions can be simplified as

$$-d\check{p}/dz + \frac{\mathrm{Gr}}{\mathrm{Re}^2} \Theta + \frac{1}{\mathrm{Re}} \nabla_s^2 W + \frac{\mathrm{Ha}^2}{\mathrm{Re}} F_z = 0, \tag{36}$$

$$\frac{1}{\mathrm{Pe}} \nabla_s^2 \Theta - W \frac{dT_m}{dz} = 0, \tag{37}$$

$$\nabla_s^2 \Phi = \nabla \cdot (v_b \times \mathbf{e}_x). \tag{38}$$

The corresponding boundary conditions on the walls are the no-slip condition for the velocity,

$$v_b = 0 \quad \text{at} \quad x = \pm 1, \quad y = \pm 1, \tag{39}$$

a fixed heat flux on the heating wall and temperature conditions on the thermal insulated sidewalls,

$$\frac{\partial \Theta}{\partial y} = -1 \quad \text{at} \quad y = -1, \tag{40}$$

$$\frac{\partial \Theta}{\partial n} = 0 \quad \text{at} \quad y = 1, \tag{41}$$

$$\frac{\partial \Theta}{\partial n} = 0 \quad \text{at} \quad x = \pm 1, \tag{42}$$

and a zero current flux due to electrically insulating walls,

$$\frac{\partial \Phi}{\partial n} = 0 \quad \text{at} \quad x = \pm 1, \quad y = \pm 1. \tag{43}$$

III. LINEAR GLOBAL STABILITY ANALYSIS

A. Numerical computation of steady mixed convection

In order to study linear global stabilities of the liquid metal mixed convection in a vertical duct, it is necessary to compute the two-dimensional steady-state solutions of the governing equations. When nonzero cross-sectional velocity is considered, the full nonlinear system of the two-dimensional governing equations, (30)–(35), can be used and solved numerically by the Newton iteration method [26]. When the cross-sectional velocity is 0, then the linear governing equations, (36)–(38), should be used. Obviously the solution of the linear governing equations must be a particular solution of the nonlinear governing equations, which may have other multiple solutions with nonzero cross-sectional velocity. It is very difficult to find the steady-state solutions with nonzero cross-sectional velocity, which require a good initial guess by the Newton iteration. Under various groups of dimensionless parameters considered in this paper, it is found that the Newton iteration always converges to the steady-state solution with zero cross-sectional velocity. Thus linear governing equations are directly used to obtain the steady-state solution for further linear stability analysis.

The steady-state solution with linear governing equations can be solved numerically by the finite-element method. A partial differential equation solver, FreeFem++ [41], with high level integration for nonlinear multiphysics systems is adopted for computation of the steady-state solutions. It is noted that in MHD duct flows the thickness of the Hartmann and Shercliff boundary layers scales as Ha^{-1} and $\mathrm{Ha}^{-1/2}$. Thus for larger Hartmann numbers, the mesh triangulations should produce a large number of dense finite elements near the four boundary walls. Such mesh triangulations are not easily realized by the FreeFem++ built-in mesh generator and can be finished manually. First, a two-dimensional nonuniform orthogonal rectangular mesh can be easily generated with Chebyshev Gauss-Lobatto collocation nodes along each coordinate direction. Then by connecting the diagonal nodes of each mesh, the rectangular mesh can be easily transformed into a triangular mesh. Kosloff-Tal-Ezer transformation is further used on the Chebyshev collocation nodes and makes the mesh nodes much closer to the boundary walls. The coordinate position for each mesh node by Kosloff-Tal-Ezer transformation is formulated as

$$x_i = \frac{\sin^{-1}(-\alpha_0 \cdot \cos(\pi i/N_x))}{\sin^{-1}\alpha_0}, \quad i = 0, \ldots, N_x,$$

$$y_j = \frac{\sin^{-1}(-\alpha_0 \cdot \cos(\pi j/N_y))}{\sin^{-1}\alpha_0}, \quad j = 0, \ldots, N_y,$$

where the parameter α_0 is a positive parameter which can control the stretching of the mesh nodes. Through computation of the most unstable eigenvalue of linear stability equations, mesh convergence has been verified by the increase in the collocation points in both coordinate directions. It is found that the mesh with $N_x = N_y = 100$ has at least three to five collocation points in the

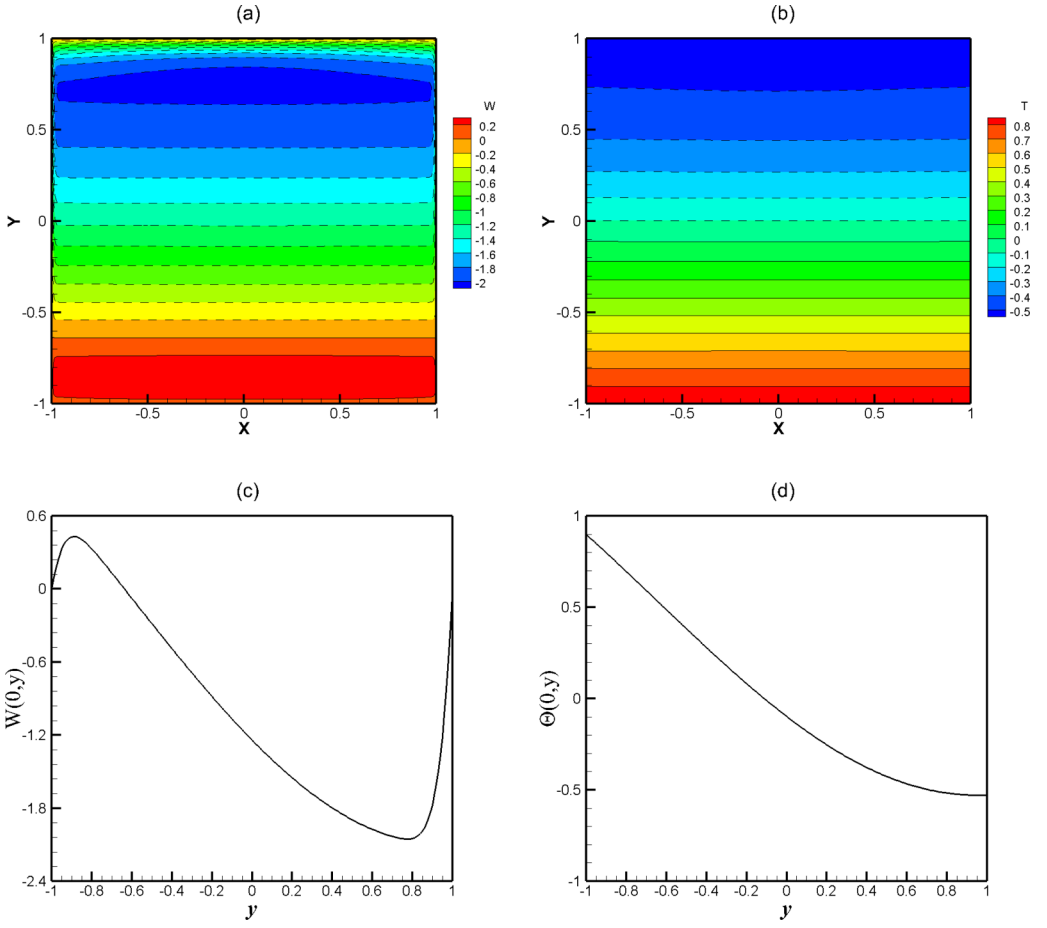

FIG. 2. Field distributions of (a, c) the streamwise velocity W and (b, d) the temperature Θ along the cross section for the steady state of the downward mixed convection flow in a vertical duct at $\mathrm{Re} = 5000$, $\mathrm{Ha} = 200$, $\mathrm{Gr} = 2\times10^6$, and $\mathrm{Pr} = 0.0321$. Solid and dashed lines in (a) and (b) represent positive and negative values, respectively.

Hartmann and Shercliff boundary layers, the most unstable eigenvalue can retain sufficient accuracy and is used henceforth for the calculations throughout the article.

Because the mean streamwise velocity is adopted as the velocity scale, it should be noted that the uniform streamwise pressure gradient $d\check{p}/dz$ should be adjusted to make the average streamwise velocity negative due to the downward flow, i.e.,

$$\frac{1}{A}\int_A W\, dA = -1. \tag{44}$$

Obviously, a simple bisection process can be used to satisfy relation (44). In actual liquid metal blankets, the LiPb eutectic alloy at a temperature of around 570 K has Prandtl number $\mathrm{Pr} = 0.0321$, while the Reynolds number may vary greatly depending on the design. In this work, several fixed Reynolds numbers are considered, $\mathrm{Re} = 2000$, 5000, and 8000, and the Grashof number and the Hartmann number are investigated in the range $10^4 \leqslant \mathrm{Gr} \leqslant 10^8$ and $10 \leqslant \mathrm{Ha} \leqslant 400$.

The steady state of the downward mixed convection flow is first computed for the field distributions of streamwise velocity W and temperature Θ along the cross section with $\mathrm{Re} = 5000$, $\mathrm{Ha} = 200$, $\mathrm{Gr} = 2\times10^6$, and $\mathrm{Pr} = 0.0321$, shown in Fig. 2. It is clearly shown that the distributions

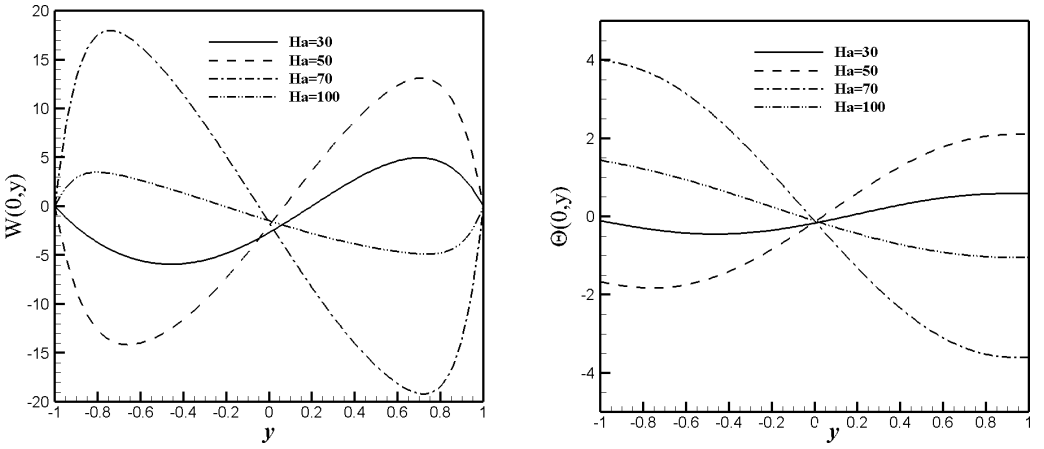

FIG. 3. Field distributions of the streamwise velocity W and temperature Θ along the middle line $x = 0$ of the cross section for the steady state of the downward mixed convection flow in a vertical duct with different Hartmann numbers at $\mathrm{Re} = 5000$, $\mathrm{Gr} = 2\times10^6$, and $\mathrm{Pr} = 0.0321$.

of the streamwise velocity and temperature field are nearly one-dimensional, i.e., $W \approx W(y)$ and $\Theta \approx \Theta(y)$. It is also shown in Figs. 2(a) and 2(c) that there exists a reversed flow near the heating wall, which may cause Kelvin-Helmholtz (KH) instability due to the appearance of an inflection point for the streamwise velocity profile. Also, a thin boundary layer appears at the opposite wall and may produce boundary layer instability. As for the temperature distribution, it is seen that the temperature decreases with an increase in the distance away from the heating wall.

It is necessary to further investigate the profile variation of the streamwise velocity and temperature field under different dimensionless parameters. As shown in Fig. 3, when the Hartmann number decreases from $\mathrm{Ha} = 100$ to $\mathrm{Ha} = 70$, the amplitudes of both upward (or reversed) and downward flows increase, and the profile of the streamwise velocity becomes more symmetrical. Thus the inflection point also moves close to the center of the duct, and the variation of the temperature field becomes larger. When the Hartmann number decreases further, to $\mathrm{Ha} = 50$, the upward (or reversed) flow near the heating wall becomes a downward flow, and also the downward flow near the opposite wall becomes an upward reverse flow. Obviously, there is a transition point Ha_t where the structure of the basic flow field changes suddenly. It should be noted that near the transition point the downward and upward flows become two strong jets with high amplitudes and opposite directions when the mechanism of KH instability must work there. Then it is very important to determine the transition point in the parameter region. Transition curves with different Reynolds numbers are plotted in Fig. 4, which is used to distinguish two different flow structures in the Ha-Gr parameter region. It is easily seen that the Hartmann number Ha_t on the transition curve becomes larger with an increase in the Grashof number. The transition curves for $\mathrm{Re} = 2000$ and $\mathrm{Re} = 8000$ are accidentally close to each other for large Grashof numbers. The region above the transition curve is labeled "up/down," which means that the flow structure in this region exhibits an upward reverse flow near the heating wall and a downward flow near the opposite wall. Conversely, the region labeled "down/up" represents that the upward reverse flow is not near the heating wall but near the opposite wall. It is also found that the transition curves would end at $\mathrm{Ha} = 0$ with a finite Grashof number below which the basic flow is always the up/down structure for any Hartmann number. Furthermore, the KH instability obviously occurs at the dimensionless parameters near the transition curve, thus the critical curve of linear stability due to the KH instability mechanism cannot cross over the transition curve and must be fully located within one of two separate regions. In the following sections, a linear global stability analysis is performed and will determine in which region the critical curve of the KH instability type is fully located.

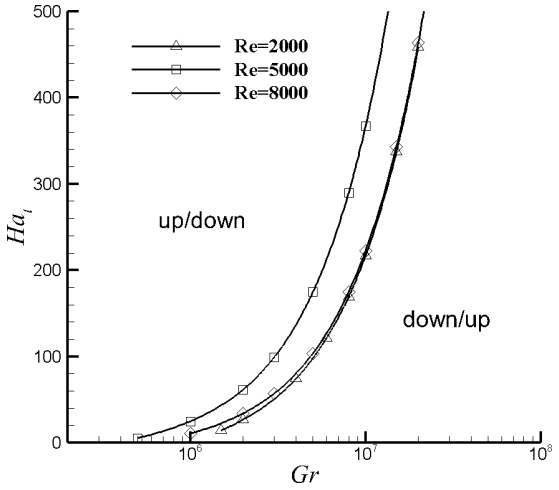

FIG. 4. Transition curves Gr-Ha$_t$ by which the parameter region is divided into two parts and two different flow structures are distinguished with different Reynolds number where Pr = 0.0321.

B. Linear global stability equations

In order to study the asymptotic behavior over time of generic low-amplitude perturbations of (V', P', Θ', Φ') imposed on steady mixed convection, these perturbations can be expanded as normal modes in the streamwise direction as

$$(V', P', \Theta', \Phi') = (\hat{v}, \hat{p}, \hat{\theta}, \hat{\phi}) \exp(ikz + \lambda t), \tag{45}$$

where k is the wave number in the streamwise direction, and $\lambda = \lambda_r + i\lambda_i$ is the corresponding complex growth rate. By substituting the expressions of the disturbed flow field $V + V'$, $P + P'$, $\Theta + \Theta'$, and $\Phi + \Phi'$ into the governing system, the full global linear stability equations are obtained as follows:

$$\lambda\hat{u} + (\overrightarrow{U} \cdot \nabla_s + ikW)\hat{u} + (\overrightarrow{\hat{u}} \cdot \nabla_s)U = -\frac{\partial \hat{p}}{\partial x} + \frac{1}{\mathrm{Re}}\left(\nabla_s^2 - k^2\right)\hat{u}, \tag{46}$$

$$\lambda\hat{v} + (\overrightarrow{U} \cdot \nabla_s + ikW)\hat{v} + (\overrightarrow{\hat{u}} \cdot \nabla_s)V = -\frac{\partial \hat{p}}{\partial y} + \frac{1}{\mathrm{Re}}\left(\nabla_s^2 - k^2\right)\hat{v} + \frac{\mathrm{Ha}^2}{\mathrm{Re}}(-ik\hat{\phi} - \hat{v}), \tag{47}$$

$$\lambda\hat{w} + (\overrightarrow{U} \cdot \nabla_s + ikW)\hat{w} + (\overrightarrow{\hat{u}} \cdot \nabla_s)W = -ik\hat{p} + \frac{1}{\mathrm{Re}}\left(\nabla_s^2 - k^2\right)\hat{w} + \frac{\mathrm{Gr}}{\mathrm{Re}^2}\hat{\theta} + \frac{\mathrm{Ha}^2}{\mathrm{Re}}\left(\frac{\partial \hat{\phi}}{\partial y} - \hat{w}\right), \tag{48}$$

$$\lambda\hat{\theta} + (\overrightarrow{U} \cdot \nabla_s + ikW)\hat{\theta} + (\overrightarrow{\hat{u}} \cdot \nabla_s)\Theta = \frac{1}{\mathrm{Pe}}\left(\nabla_s^2 - k^2\right)\hat{\theta} - \hat{w}\frac{dT_m}{dz}, \tag{49}$$

$$\frac{\partial \hat{u}}{\partial x} + \frac{\partial \hat{v}}{\partial y} + ik\hat{w} = 0, \tag{50}$$

$$\left(\nabla_s^2 - k^2\right)\hat{\phi} - \left(\frac{\partial \hat{w}}{\partial y} - ik\hat{v}\right) = 0. \tag{51}$$

Here, $\hat{v} = (\overrightarrow{\hat{u}}, \hat{w}) = (\hat{u}, \hat{v}, \hat{w})$. And the boundary conditions are given by

$$\hat{v} = \frac{\partial \hat{\theta}}{\partial n} = \frac{\partial \hat{\phi}}{\partial n} = 0 \quad \text{at} \quad y = \pm 1 \quad \text{or} \quad x = \pm 1. \tag{52}$$

The spatial discretization of the Taylor-Hood finite element can be used for the global linear stability equations. After the spatial discretization of the linear stability equations, a generalized eigenvalue problem has to be solved in the matrix form as

$$A\hat{q} = \lambda B\hat{q}, \tag{53}$$

where $\hat{q} = (\hat{v}, \hat{p}, \hat{\theta}, \hat{\phi})$ is the eigenvector collecting the velocity components, pressure, temperature, and electrostatic potential on each degree of freedom of the discrete problem, and A and B are large sparse complex matrices.

In order to facilitate the extraction of the desired eigenvalues for unstable modes, spectral transformations should be introduced into the generalized eigenvalue problem. Theofilis [42] has reviewed a lot of spectral transformations commonly utilized in global instability analysis of fluid flows. Most commonly used is the shift-and-invert strategy, which transforms the generalized eigenvalue problem into a standard eigenvalue problem as follows:

$$(A - \mu B)^{-1} B\hat{q} = (\lambda - \mu)^{-1}\hat{q}. \tag{54}$$

The shift matrix can be solved by UMFPACK or the MUMPS sparse LU solver and the standard eigenvalue problem solved with an implicitly restarted Arnoldi algorithm as provided in the ARPACK software library [43]. Thus, the largest eigenvalues of the transformed matrix now correspond to those eigenvalues of the original generalized eigenvalue equation which are the closest to the shift value μ.

C. Elevator unstable mode

Elevator modes driven by a vertical temperature gradient are in fact two-dimensional instability modes with $k = 0$, as well as $\hat{u} = \hat{v} = 0$. Then the two-dimensional stability equations for the elevator modes are represented as

$$\lambda\hat{w} = \frac{1}{\mathrm{Re}}\nabla_s^2\hat{w} + \frac{\mathrm{Gr}}{\mathrm{Re}^2}\hat{\theta} + \frac{\mathrm{Ha}^2}{\mathrm{Re}}\left(\frac{\partial\hat{\phi}}{\partial y} - \hat{w}\right), \tag{55}$$

$$\lambda\hat{\theta} = \frac{1}{\mathrm{Pe}}\nabla_s^2\hat{\theta} - \hat{w}\frac{dT_m}{dz}, \tag{56}$$

$$\nabla_s^2\hat{\phi} - \frac{\partial\hat{w}}{\partial y} = 0. \tag{57}$$

Obviously, elevator modes have nothing to do with the basic flow field structure but can change the field structure greatly. Through the eigenvalue computation of the two-dimensional stability equations, only one unstable branch of elevator modes is found and its exponential growth rate λ_r as a function of the Grashof number Gr is plotted with different Hartmann numbers at $\mathrm{Re} = 5000$ and $\mathrm{Pr} = 0.0321$, as shown in Fig. 5. In this figure, it is easily seen that with an increase in the Grashof number the growth rate of the unstable elevator mode increases continuously. Meanwhile, at the same Grashof number a larger Hartmann number has a lower growth rate, thus the magnetic field has a stabilization effect on the unstable elevator mode. It also seems that when the Grashof number approaches 0, i.e., $\mathrm{Gr} \to 0$, the growth rate approaches close to 0 for all Hartmann numbers. Moreover, the growth rate of the unstable elevator mode is always positive and never found to fall below 0 for the whole dimensionless parameters considered in this paper. The two-dimensional unstable elevator mode is revealed to be stationary due to the zero angular frequency ($\lambda_i = 0$), which is not shown here.

The spatial structure of the unstable elevator mode with respect to the streamwise velocity $\hat{w}$ and temperature $\hat{\theta}$ in the cross section is shown in Fig. 6. Due to the independence of the unstable elevator mode in the basic flow profile, both the streamwise velocity $\hat{w}$ and temperature $\hat{\theta}$ are symmetrical with respect to the axes $x = 0$ and $y = 0$. Thus the growth of the unstable elevator mode may symmetrically and locally change the up/down or down/up flow structure greatly and,

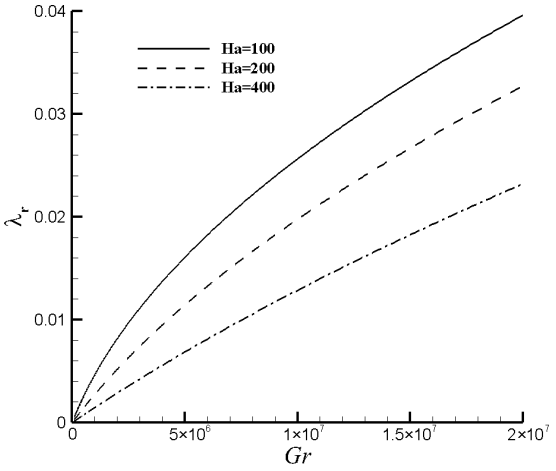

FIG. 5. The growth rate of the most unstable elevator mode as a function of the Grashof number Gr with different Hartmann numbers at Re = 5000 and Pr = 0.0321.

also, may evolve into jets with a significant amplitude. Furthermore, secondary instabilities may appear during the evolution of the unstable elevator mode. Early studies mainly took the elevator mode as the main physical mechanism for experimental and numerical simulation results. However, it is shown in the next section that there exists a three-dimensional oscillatory (or traveling) mode which also can be a physical unstable mechanism for these results.

D. Three-dimensional oscillatory instability

Three-dimensional instabilities occur at a nonzero wave number along with a zero or nonzero angular frequency (stationary or oscillatory instability). For a downward MHD mixed convection flow in the vertical duct, a three-dimensional oscillatory unstable mode is found and its linear growth rate and angular frequency as a function of the wave number are plotted in Fig. 7 for different Hartmann numbers with Re = 5000, Gr = 2×10^6, and Pr = 0.0321. It is clearly shown that the most unstable growth rate and its corresponding wave number decrease with an increase in the Hartmann number. This demonstrates that a stronger magnetic field has a much stronger stabilization effect, especially for short-wave perturbation, thus a large enough Hartmann number

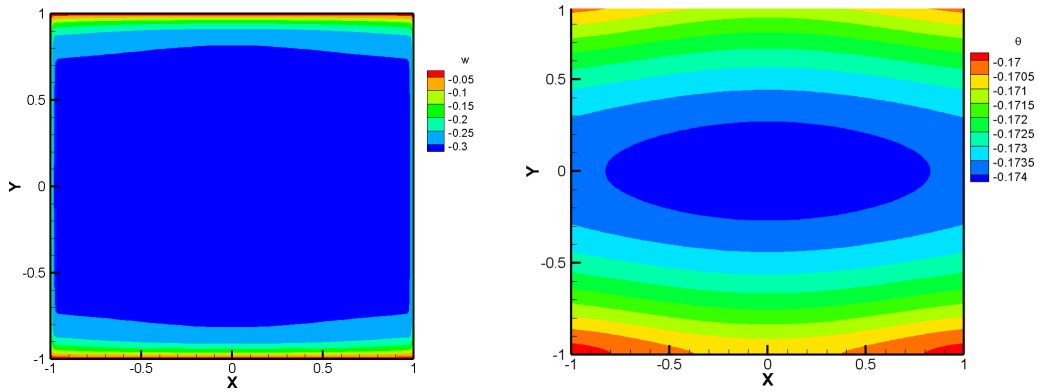

FIG. 6. The spatial structure of the unstable elevator mode with respect to the streamwise velocity $\hat{w}$ and temperature $\hat{\theta}$ in the cross section at Re = 5000, Ha = 200, Gr = 2×10^6, and Pr = 0.0321.

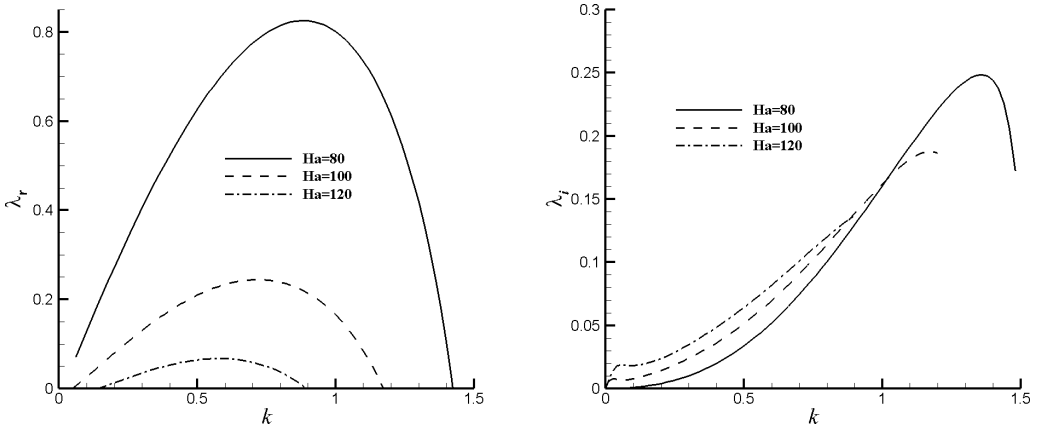

FIG. 7. The linear growth rate λ_r and angular frequency λ_i of the three-dimensional oscillatory unstable mode as a function of the wave number k for different Hartmann numbers at $\mathrm{Re} = 5000$, $\mathrm{Gr} = 2\times10^6$, and $\mathrm{Pr} = 0.0321$.

can make the oscillatory mode stable. The angular frequency is always positive and increases with the wave number for the unstable region. A positive angular frequency means that the traveling wave of the oscillatory mode propagates downward in the vertical duct.

To study the critical stability boundary of the three-dimensional oscillatory mode, it is necessary to plot the critical curves for both the Grashof number Gr_c and the wave number as a function of the Hartmann number for different Reynolds numbers, as shown in Fig. 8. From the critical curves of Gr_c-Ha, it is easily seen that with an increase in the Hartmann number the critical Grashof number increases more slowly for a small Hartmann number, then after $\mathrm{Ha} = 120$ it increases more rapidly and shows linear growth. With a further increase in the Hartmann number, it seems that the critical value of $\mathrm{Gr}_c/(\mathrm{Ha}\,\mathrm{Re})$ approaches a constant finite value around 4.5, which can be compared to the threshold value of around 4 given by the numerical simulations of Zhang and Zikanov [32]. It is also found that at the same Hartmann number, a higher Reynolds number has a larger critical Grashof

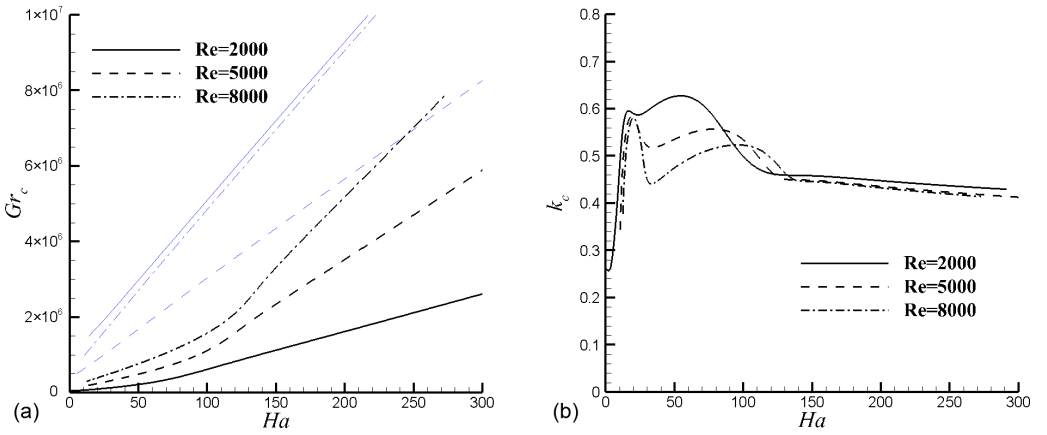

FIG. 8. (a) The critical Grashof number Gr_c and (b) the critical wave number k_c as a function of the Hartmann number for the three-dimensional oscillatory mode of the MHD mixed convection flow for different Reynolds numbers with $\mathrm{Pr} = 0.0321$. Here, thick lines represent critical curves, and thin blue lines transition curves in Fig. 4.

number. The transition curves for the structure change of basic flow are also plotted and located above the corresponding critical curves. Obviously, the critical curves are located in the up/down region and this shows that the first instability of the oscillatory mode occurs at the basic MHD mixed convection with an upward reverse flow near the heating wall and a downward flow near the opposite wall. It is also noted that for a larger Reynolds number the critical curve of the Grashof number is much closer to the transition curve of the basic flow structure.

Returning to the critical wave number k_c shown in Fig. 8(b), we can see that for small Hartmann numbers there exists an oscillatory change in the critical wave number, such as from a small value ($\approx$0.3) at Ha = 10 quickly to a large value ($\approx$0.58) at Ha = 18. The oscillatory change stops near Ha = 130, and then the critical wave number begins to decrease slowly. It is interesting to see that the critical wave numbers of Re = 5000 and Re = 8000 are very close at the same large Hartmann number. This implicitly indicates that for a strong magnetic field and larger basic average streamwise velocity the perturbations at the critical point have almost the same wavelength.

The spatial structures of three-dimensional oscillatory modes can be further given at a fixed time from the eigenvectors at the critical point ($\lambda_r = 0$). If the discretized eigenvector is denoted $X = X_r + iX_i$, the perturbation at wave number k and angular frequency λ_i is obtained by $\mathrm{Re}(Xe^{i(kz+\lambda_i t)})$, where Re denotes the real part. The spatial structure of the three-dimensional oscillatory mode in the midplane section $x = 0$ of the vertical duct is plotted in Fig. 9 for the perturbations of the transverse velocity in the y direction, the streamwise velocity in the z direction, the vorticity component in the x direction, and the temperature at a critical point of $k_c = 0.4358$, Gr = 3 530 593.55 with Re = 5000, Ha = 200, and Pr = 0.0321. It is easily seen that the perturbations with a high amplitude are concentrated mainly in three regions. From the spatial distributions of the vorticity component in the x direction and the temperature, one region is located near the inflection point of the streamwise velocity profile $W(0, y)$, i.e., $\partial^2 W(0, y_i)/\partial y^2 = 0$ with $y_i \approx -0.25$ for the critical parameters considered here. The perturbations near the inflection point may be attributed to the mechanism of KH instability. From spatial distributions of the streamwise velocity in the z direction and the vorticity component in the x direction, the other two regions with large perturbations are situated close to the heating wall and its opposite wall. The spatial perturbation distribution within these regions also may produce the boundary layer instability. The existence of the KH instability and boundary layer instability is further validated by energy budget analyses in the following subsection.

E. Energy budget analyses

In order to gain deep physical insight into the destabilization mechanism in the oscillatory unstable mode, it is necessary to perform energy budget analyses at the critical thresholds. First, the linear stability equations, (46)–(48), are multiplied by the complex conjugate of the velocity perturbation $\hat{v}^*$ and then integrated in the cross section A. After some simplifications, an equation giving the rate of change of the fluctuating kinetic energy can be derived. At the critical threshold [$\mathrm{Re}(\lambda) = 0$] for any unstable mode, kinetic energy budgets can be further obtained as

$$E_{\mathrm{su}} + E_{\mathrm{sv}} + E_{\mathrm{sw}} + E_b + E_m + E_d = 0, \tag{58}$$

where E_{su}, E_{sv}, and E_{sw} are the productions of fluctuating kinetic energy by shear of the basic flow, E_b is the production of fluctuating kinetic energy by buoyancy, E_m is the dissipation of fluctuating kinetic energy by magnetic forces, and E_d is the viscous dissipation of fluctuating kinetic energy. They are defined as follows:

$$E_{\mathrm{su}} = -\mathrm{Re}\left(\int_A \left[\hat{u}\frac{\partial U}{\partial x}\hat{u}^* + \hat{v}\frac{\partial U}{\partial y}\hat{u}^*\right] dxdy\right), \tag{59}$$

$$E_{\mathrm{sv}} = -\mathrm{Re}\left(\int_A \left[\hat{u}\frac{\partial V}{\partial x}\hat{v}^* + \hat{v}\frac{\partial V}{\partial y}\hat{v}^*\right] dxdy\right), \tag{60}$$

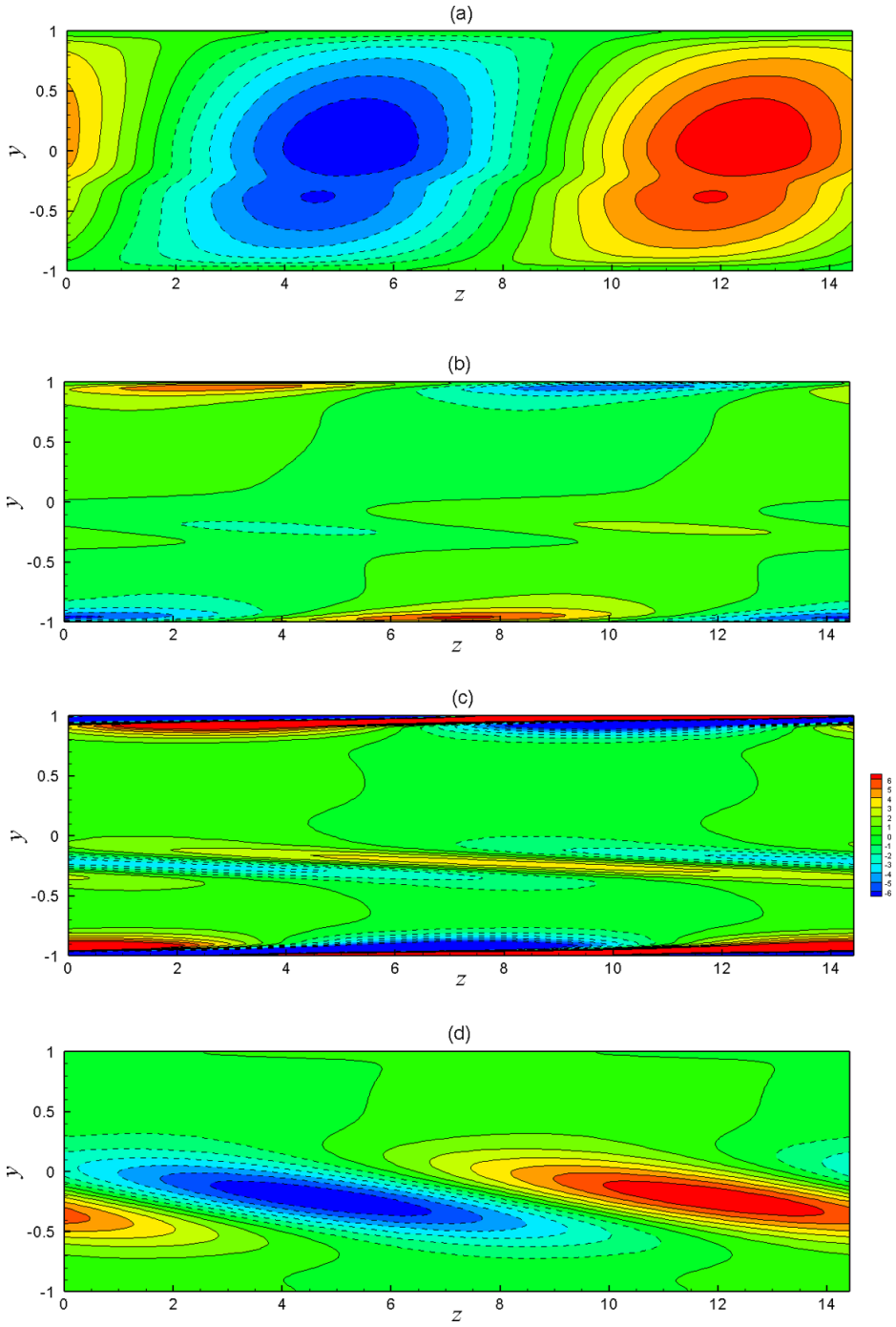

FIG. 9. Spatial structure of the three-dimensional oscillatory mode in the midplane section $x = 0$ of the vertical duct for the perturbations of the transverse velocity in the y direction (top row), the streamwise velocity in the z direction (second row), the vorticity component in the x direction (third row), and the temperature (bottom row) at a critical point of $k_c = 0.4358$, $\mathrm{Gr} = 3\,530\,593.55$ with $\mathrm{Re} = 5000$, $\mathrm{Ha} = 200$, and $\mathrm{Pr} = 0.0321$.

TABLE I. Kinetic energy budgets by the streamwise shear of the basic flow E'_{sw}, buoyancy E'_b, and magnetic forces E'_m at the critical point of the three-dimensional oscillatory unstable mode for different Reynolds numbers and Hartmann numbers with Pr = 0.0321.

Re	Ha	Gr_c	k_c	E'_{sw}	E'_b	E'_m
2000	50	219949.01	0.626	1.2053	−0.0082	−0.1971
	100	620747.06	0.499	1.1641	0.0634	−0.2275
	200	1622045.47	0.448	1.1129	0.1465	−0.2593
	300	2617396.99	0.428	1.0811	0.2132	−0.2942
5000	50	491881.52	0.536	1.1503	0.0117	−0.1620
	100	1118677.51	0.534	1.1932	−0.0026	−0.1905
	200	3530593.55	0.436	1.1110	0.0931	−0.2040
	300	5901688.88	0.413	1.0952	0.1341	−0.2292
8000	50	768284.31	0.475	1.1340	0.0167	−0.1506
	100	1584341.48	0.523	1.1830	−0.0124	−0.1705
	200	5189962.83	0.433	1.1079	0.0730	−0.1808
	250	7030357.09	0.419	1.1047	0.0856	−0.1902

$$E_{sw} = -\mathrm{Re}\left(\int_A \left[\hat{u}\frac{\partial W}{\partial x}\hat{w}^* + \hat{v}\frac{\partial W}{\partial y}\hat{w}^*\right] dxdy\right), \tag{61}$$

$$E_b = \mathrm{Re}\left(\int_A \frac{\mathrm{Gr}}{\mathrm{Re}^2}\hat{\theta}\hat{w}^*\, dxdy\right), \tag{62}$$

$$E_m = \mathrm{Re}\left(\int_A \frac{\mathrm{Ha}^2}{\mathrm{Re}}[(-\nabla\hat{\phi} + \hat{v}\times\mathbf{e}_x)\times\mathbf{e}_x]\hat{v}^*\, dxdy\right), \tag{63}$$

$$E_d = -\mathrm{Re}\left(\int_A \frac{1}{\mathrm{Re}}\frac{\partial\hat{v}_i}{\partial x_j}\frac{\partial\hat{v}_i^*}{\partial x_j}\, dxdy\right). \tag{64}$$

Due to the zero cross-sectional velocity ($U = V = 0$) for the basic flow, the production of fluctuating kinetic energy from the cross-sectional shear of the basic flow is 0, i.e., $E_{su} = 0$ and $E_{sv} = 0$. All other terms can be further normalized by the viscous dissipation of fluctuating kinetic energy E_d, then a normalized kinetic energy budget equation is written as

$$E'_{sw} + E'_b + E'_m = 1, \tag{65}$$

where $E'_{sw} = E_{sw}/|E_d|$, $E'_b = E_b/|E_d|$, and $E'_m = E_m/|E_d|$.

The kinetic energy budgets by shear of the basic flow, buoyancy, and magnetic forces at the critical points of the three-dimensional oscillatory unstable mode are presented for different Reynolds numbers and Hartmann numbers in Table I. It is easily seen that in all cases the production of fluctuating kinetic energy by the streamwise shear of the basic flow E_{sw} is the dominant destabilizing term, which is comparable to the stabilizing viscous dissipation term. The magnetic term E_m is always negative and has an obvious stabilization effect on the flow system. When the magnetic field is not very strong such as Ha = 50 or 100, it is found that the buoyancy term E_b has only a minor impact on the production of fluctuating kinetic energy. However, with an increase in the magnetic field such as Ha = 200 or 300, the buoyancy term E_b becomes comparable to the magnetic term E_m and has a more and more obvious destabilization effect.

Now the three-dimensional oscillatory unstable mode can be attributed to the shear instability mechanism due to the dominant destabilizing term by the streamwise shear of the basic flow for the production of fluctuating kinetic energy. However, both KH instability and boundary layer instability belong to shear instabilities, thus it is not clear which one will play a leading role. To this end, we can look into the integral terms in the integral formulas, (63) and (64), which represent the local

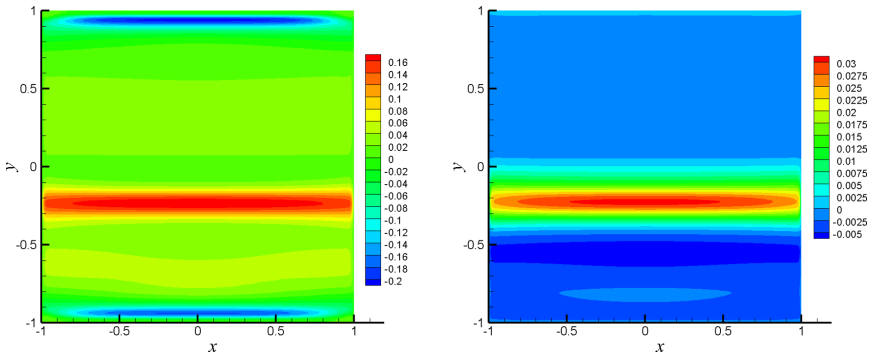

FIG. 10. Spatial distribution of the local streamwise shear of the basic flow E'_{sw} and local buoyancy E'_b at a critical point of the three-dimensional oscillatory unstable mode with $\mathrm{Re} = 5000$, $\mathrm{Ha} = 200$, $\mathrm{Gr}_c = 3\,530\,593.55$, $k_c = 0.436$, and $\mathrm{Pr} = 0.0321$.

production of fluctuating kinetic energy due to the local streamwise shear of the basic flow and local buoyancy, respectively. The spatial distribution of the local streamwise shear of the basic flow and local buoyancy is plotted in Fig. 10 at the critical point of $\mathrm{Re} = 5000$ and $\mathrm{Ha} = 200$. It is clearly seen that the local streamwise shear of the basic flow is positive around the inflection line $y_i \approx -0.25$ but is negative near the two opposite walls perpendicular to the direction of the heat flux. It is also found that the positive local buoyancy is distributed around the same inflection line. This means that there exists only the KH instability without the boundary layer instability for the parameters considered here. Thus the three-dimensional oscillatory unstable mode originates in the KH instability mechanism due to the existence of an inflection point.

F. Remark on the elevator mode and oscillatory mode

Unstable elevator and oscillatory modes have been found for the downward flow of liquid metal in a vertical duct under strong wall heating and a transverse magnetic field. There exists a critical curve for the oscillatory mode, while the elevator mode is found to be always unstable. Thus we are concerned with the growth strength of the elevator mode when the oscillation mode becomes unstable. We put the critical curve Ha-Gr_c of the oscillatory mode and contour lines of the linear growth rate of the elevator mode together, as shown in Fig. 11. It is clearly shown that when the oscillation mode becomes unstable for $\mathrm{Ha} < 100$, the elevator mode has a growth rate between 0.001 and 0.005. When $100 < \mathrm{Ha} < 300$ the growth rate of the elevator mode is between 0.005 and 0.01, while for $\mathrm{Ha} > 300$ the growth rate of the elevator mode is larger than 0.01. Thus with an increase in the Hartmann number along the critical curve of the oscillatory mode, the elevator mode becomes much more unstable. So the elevator mode will always play an important role whether or not an unstable oscillatory mode exists.

IV. CONCLUSION

Unstable elevator and oscillatory modes are revealed through linear global stability analysis of the downward flow of liquid metal in a vertical duct under strong wall heating and a transverse magnetic field. The elevator mode is found to be always unstable, while the oscillatory mode becomes unstable above a critical curve of Ha-Gr_c for different Reynolds numbers under a specific flow structure which exhibits an upward reverse flow near the heating wall and a downward flow near the opposite wall. Below the critical Grashof number of the unstable oscillatory mode, the unstable elevator mode plays a major role through its first growth to a significant amplitude, and then the flow field may experience secondary instabilities and break down into three-dimensional fluctuations. Such an evolution process induced by the elevator mode has been used [39] to explain the high-

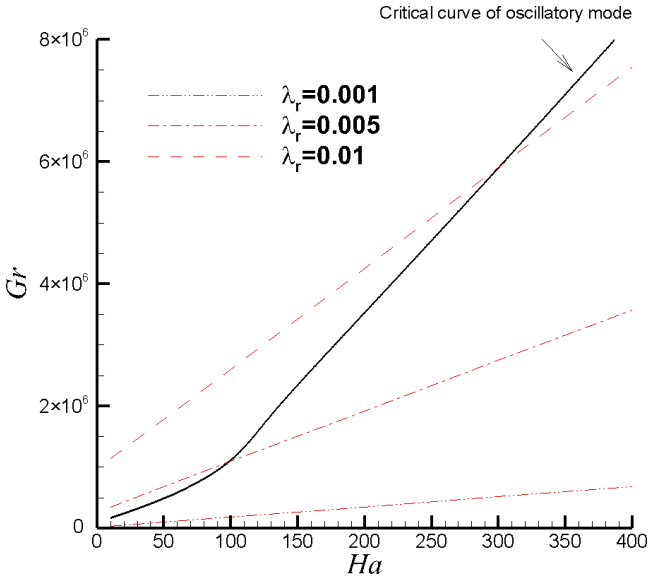

FIG. 11. Critical curve Ha-Gr_c of the oscillatory mode (thick solid line) and contour lines of the linear growth rate of the elevator mode (thin red lines), where Re = 5000 and Pr = 0.0321.

amplitude, low-frequency pulsations of temperature in the form of isolated bursts or quasiregular fluctuations in direct numerical simulations [31,40] and experiments [29,30]. However, above the critical Grashof number, as a new discovery of the destabilization mechanism, the three-dimensional unstable oscillatory mode will play an important role together with the elevator mode. If initial perturbations are small, perturbations of both the elevator and the oscillatory mode will increase at the same time. When the perturbations are large enough, a nonlinear effect should be considered. Thus a weak nonlinear analysis of the two unstable modes is worthy of further study and used for a new explanation of high-amplitude low-frequency pulsations.

Energy budget analyses of the three-dimensional oscillatory mode were further carried out at the critical thresholds of different Reynolds numbers and Hartmann numbers and revealed that the streamwise shear of the basic flow is the the dominant destabilizing term for the production of fluctuating kinetic energy. The buoyancy term has a notable destabilization effect only for large Hartmann numbers, while the magnetic term always has an obvious stabilization effect for any magnetic field intensity. Meanwhile, it is verified that the shear KH instability due to the existence of an inflection point is the key instability mechanism of the three-dimensional oscillatory mode.

ACKNOWLEDGMENT

This work was supported by the National Natural Science Foundation of China (Grant No. 11672046).

[1] M. Abdou, D. Sze, C. Wong, M. Sawan, A. Ying, N. B. Morley, and S. Malang, U.S. plans and strategy for ITER blanket testing, Fusion Sci. Technol. **47**, 475 (2005).

[2] S. Malang, M. Tillack, C. P. C. Wong, N. Morley, and S. Smolentsev, Development of the lead lithium (DCLL) blanket concept, Fusion Sci. Technol. **60**, 249 (2011).

[3] M. Abdou, N. B. Morley, S. Smolentsev, A. Ying, S. Malang, A. Rowcliffe, and M. Ulrickson, Blanket/first wall challenges and required R&D on the pathway to DEMO, Fusion Eng. Des. **100**, 2 (2015).

[4] S. Smolentsev, N. B. Morley, M. A. Abdou, and S. Malang, Dual-coolant lead-lithium (DCLL) blanket status and R&D needs, Fusion Eng. Des. **100**, 44 (2015).
[5] L. M. Giancarli, X. Bravo, S. Cho, M. Ferrari, T. Hayashi, B.-Y. Kim, A. Leal-Pereira, J.-P. Martins, M. Merola, R. Pascal, I. Schneiderova, Q. Sheng, A. Sircar, Y. Strebkov, J. van der Laan, and A. Ying, Overview of recent ITER TBM program activities, Fusion Eng. Des. **158**, 111674 (2020).
[6] S. Molokov, R. Moreau, and H. K. Moffatt, *Magnetohydrodynamics: Historical Evolution and Trends* (Springer, Berlin, 2007).
[7] P. H. Roberts, *An Introduction to Magnetohydrodynamics* (Longman, Harlow, UK, 1967).
[8] U. Müller and L. Bühler, *Magnetohydrodynamics in Channels and Containers* (Springer, Berlin, 2001).
[9] P. A. Davidson, *An Introduction to Magnetohydrodynamics* (Cambridge University Press, Cambridge, UK, 2001).
[10] H. K. Moffatt, On the suppression of turbulence by a uniform magnetic field, J. Fluid Mech. **28**, 571 (1967).
[11] P. A. Davidson, Magnetic damping of jets and vortices, J. Fluid Mech. **299**, 153 (1995).
[12] V. Shatrov and G. Gerbeth, Marginal turbulent magnetohydrodynamic flow in a square duct, Phys. Fluids **22**, 084101 (2010).
[13] O. Zikanov, D. Krasnov, T. Boeck, A. Thess, and M. Rossi, Laminar-turbulent transition in magnetohydrodynamic duct, pipe, and channel flows, Appl. Mech. Rev. **66**, 030802 (2014).
[14] B. Lehnert, On the behaviour of an electrically conductive liquid in a magnetic field, Ark. Fys. **5**, 69 (1952).
[15] T. Kakutani, The hydrodynamic stability of the modified plane couette flow in the presence of a transverse magnetic field, J. Phys. Soc. Jpn. **19**, 1041 (1964).
[16] J. C. R. Hunt, Magnetohydrodynamic flow in rectangular ducts, J. Fluid Mech. **21**, 577 (1965).
[17] J. Priede, S. Aleksandrova, and S. Molokov, Linear stability of hunt's flow, J. Fluid Mech. **649**, 115 (2010).
[18] J. Priede, S. Aleksandrova, and S. Molokov, Linear stability of magnetohydrodynamic flow in a perfectly conducting rectangular duct, J. Fluid Mech. **708**, 111 (2012).
[19] J. Priede, T. Arlt, and L. Bühler, Linear stability of magnetohydrodynamic flow in a square duct with thin conducting walls, J. Fluid Mech. **788**, 129 (2015).
[20] P. Moresco and T. Alboussire, Experimental study of the instability of the Hartmann layer, J. Fluid Mech. **504**, 167 (2004).
[21] M. Kinet, B. Knaepen, and S. Molokov, Instabilities and Transition in Magnetohydrodynamic Flows in Ducts with Electrically Conducting Walls, Phys. Rev. Lett. **103**, 154501 (2009).
[22] L. G. Genin, V. G. Zhilin, Y. P. Ivochkin, N. G. Razuvanov, I. A. Belyaev, Y. I. Listratov, and V. G. Sviridov, Temperature fluctuations in a heated horizontal tube affected by transverse magnetic field, in *Proceedings of the 8th PAMIR International Conference on Fundamental and Applied MHD, Borgo, Corsica, France* (2011), pp. 37–41.
[23] I. A. Belyaev, Y. P. Ivochkin, Y. I. Listratov, N. G. Razuvanov, and V. G. Sviridov, Temperature fluctuations in a liquid metal mhd-flow in a horizontal inhomogeneously heated tube, High Temp. **53**, 734 (2015).
[24] O. Zikanov, Y. I. Listratov, and V. G. Sviridov, Natural convection in horizontal pipe flow with a strong transverse magnetic field, J. Fluid Mech. **720**, 486 (2013).
[25] X. Zhang and O. Zikanov, Mixed convection in a horizontal duct with bottom heating and strong transverse magnetic field, J. Fluid Mech. **757**, 33 (2014).
[26] J. Hu, Linear global stability of liquid metal mixed convection in a horizontal bottom-heating duct under strong transverse magnetic field, Phys. Fluids **32**, 034108 (2020).
[27] I. R. Kirillov, D. M. Obukhov, L. G. Genin, V. G. Sviridov, N. G. Razuvanov, V. M. Batenin, I. A. Belyaev, I. I. Poddubnyi, and N. Yu Pyatnitskaya, Buoyancy effects in vertical rectangular duct with coplanar magnetic field and single sided heat load, Fusion Eng. Des. **104**, 1 (2016).
[28] Ya. Listratov, I. Melnikov, N. Razuvanov, V. Sviridov, and O. Zikanov, Convection instability and temperature fluctuations in a downward flow in a vertical pipe with strong transverse magnetic field, in

Proceedings of the 10th PAMIR Conference Fundamental and Applied MHD (INP, Open Library, Cagliari, Italy, 2016), Vol. 1.

[29] I. A. Melnikov, E. V. Sviridov, V. G. Sviridov, and N. G. Razuvanov, Heat transfer of MHD flow: Experimental and numerical research, in *Proceedings of the 9th PAMIR Conference Fundamental and Applied MHD* (INP, Open Library, Riga, Latvia, 2014), Vol. 1, pp. 65–69.

[30] I. A. Melnikov, E. V. Sviridov, V. G. Sviridov, and N. G. Razuvanov, Experimental investigation of MHD heat transfer in a vertical round tube affected by transverse magnetic field, Fusion Eng. Des. **112**, 505 (2016).

[31] I. Belyaev, D. Krasnov, Y. Kolesnikov, D. Biryukov, D. Chernysh, O. Zikanov, and Y. Listratov, Effects of symmetry on magnetohydrodynamic mixed convection flow in a vertical duct, Phys. Fluids **32**, 094106 (2020).

[32] X. Zhang and O. Zikanov, Convection instability in a downward flow in a vertical duct with strong transverse magnetic field, Phys. Fluids **30**, 117101 (2018).

[33] I. Belyaev, P. Sardov, I. Melnikov, and P. Frick, Limits of strong magneto-convective fluctuations in liquid metal flow in a heated vertical pipe affected by a transverse magnetic field, Int. J. Therm. Sci. **161**, 106773 (2021).

[34] O. Zikanov, I. Belyaev, Y. Listratov, P. Frick, N. Razuvanov, and P. Sardov, Mixed convection in pipe and duct flows with strong magnetic fields, Appl. Mech. Rev. **73**, 010801 (2021).

[35] J. Sommeria and R. Moreau, Why, how, and when, MHD turbulence becomes two-dimensional, J. Fluid Mech. **118**, 507 (1982).

[36] S. Smolentsev, N. Vetcha, and R. Moreau, Study of instabilities and transitions for a family of quasi-two-dimensional magnetohydrodynamic flows based on a parametrical model, Phys. Fluids **24**, 024101 (2012).

[37] N. Vetcha, S. Smolentsev, M. Abdou, and R. Moreau, Study of instabilities and quasi-two-dimensional turbulence in volumetrically heated magnetohydrodynamic flows in a vertical rectangular duct, Phys. Fluids **25**, 024102 (2013).

[38] T. Vo, A. Pothérat, and G. J. Sheard, Linear stability of horizontal, laminar fully developed, quasi-two-dimensional liquid metal duct flow under a transverse magnetic field and heated from below, Phys. Rev. Fluids **2**, 033902 (2017).

[39] L. Liu and O. Zikanov, Elevator mode convection in flows with strong magnetic fields, Phys. Fluids **27**, 044103 (2015).

[40] O. Zikanov and Y. Listratov, Numerical investigation of MHD heat transfer in a vertical round tube affected by transverse magnetic field, Fusion Eng. Design **113**, 151 (2016).

[41] O. Pironneau, F. Hecht, and J. Morice, *Freefem++*; available at: http://www.freefem.org (2013).

[42] V. Theofilis, Global linear instability, Annu. Rev. Fluid Mech. **43**, 319 (2011).

[43] R. Lehoucq, D. Sorensen, and C. Yang, *Arpack Users' Guide: Solution of Large-Scale Eigenvalue Problems with Implicitly Restarted Arnoldi Methods* (SIAM, Philadelphia, 1998).